THE JOURNAL OF PHYSICAL CHEMISTRY B

ARTICLE

pubs.acs.org/JPCB

Computational Evidence for α-Nitrosamino Radical as Initial Metabolite for Both the P450 Dealkylation and Denitrosation of Carcinogenic Nitrosamines

Li Ji and Gerrit Schüürmann*

UFZ Department of Ecological Chemistry, Helmholtz Centre for Environmental Research, Permoserstrasse 15, 04318 Leipzig, Germany, and Institute for Organic Chemistry, Technical University Bergakademie Freiberg, Leipziger Strasse 29, 09596 Freiberg, Germany

Supporting Information

ABSTRACT: The mutagenic and carcinogenic potency of α-CH_n-nitrosamines such as *N*-nitrosodimethylamine (NDMA) is caused by their P450-catalyzed α-hydroxylation and subsequent dealkylation, yielding alkyl diazonium ions ($R-N\equiv N^+$) as potent electrophiles. Alternatively, P450s may also catalyze their denitrosation as metabolic detoxification. DFT calculations at the UB3LYP/LANL2DZ(Fe)/6-31G+**(H,C,N,O,S)//LANL2DZ(Fe)/6-31G(H,C,N,O,S) level of theory show that H-abstraction from the α-C of NDMA as initial metabolic step yields an α-nitrosamino radical ($\bullet CH_2N(CH_3)NO$) as common first intermediate for both the oxidative dealkylation (toxification) and denitrosation (detoxification) pathways. In particular, the calculated kinetic isotope effect for the P450-mediated dealkylation of NDMA is in good agreement with experimental information. The results show further that the initial α-hydroxylation of NDMA may proceed in two spin states. Besides a stepwise high-spin (HS, quartet) route with a separate rebound barrier, there is a concerted low-spin (LS, doublet) pathway. Interestingly, the resultant two-state reactivity appears to discriminate between metabolic toxification and detoxification: Evaluation of calculated free energy barriers of the H-abstraction ($\Delta G^{\ddagger}$) through the Eyring equation suggests that the dealkylation:denitrosation product ratio is governed by the LS:HS ratio of the overall metabolic process. Moreover, inclusion of three further α-CH_n-nitrosamines in the computational analysis demonstrates that the initial H-abstraction barrier is proportional to the C−H bond dissociation enthalpy (BDE) of the substrates, which enables the estimation of spin-averaged reaction barriers through ground-state BDE calculations. The discussion includes also reductive denitrosation pathways that according to current computational evidence appear to be unlikely for aliphatic nitrosamines.

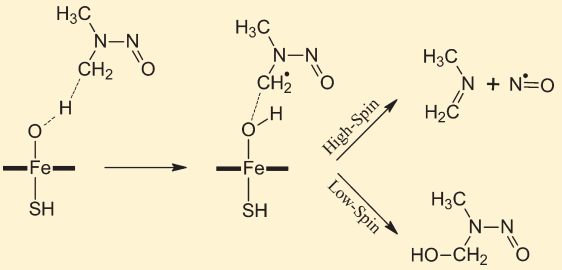

INTRODUCTION

The C−H hydroxylation by cytochrome P450 enzymes (P450s) is quite common in the metabolism of steroids, fatty acids, and aliphatic hydrocarbons.[1] However, this metabolic conversion may also initiate the conversion of xenobiotics to carcinogenic electrophiles.[2] A prominent example is given by the P450-mediated α-hydroxylation of nitrosamines, leading to alkyl diazonium ions or carbenium ions as ultimate DNA-reactive carcinogens.[3] The α-hydroxylation process is believed to involve an initial hydrogen abstraction and its transfer to the P450 Fe=O moiety because of high kinetic deuterium isotope effects (KIE) measured for the N-dealkylation of nitrosamines.[4,5]

Subsequent toxification proceeds through recombination of the accordingly generated α-nitrosamino radical with •OH from FeOH, yielding an α-hydroxynitrosamine that can release a carbonyl and OH^- to form an alkyl diazonium ion.[6] The latter represents the ultimate carcinogen, attacking DNA bases through an S_N2 mechanism (the alternative S_N1 route through release of N_2 yielding CH_3^+ as critical electrophile is less likely because of its high energy).

Alternatively, P450s can also catalyze the denitrosation as detoxification of nitrosamines, preventing their transformation to ultimate carcinogens. Here, the initially formed α-nitrosamino radical may fragment to nitric oxide and imine, followed by hydrolysis to an aldehyde and methylamine in the denitrosation route of *N*-nitrosodimethylamine (NDMA).[5] Both the dealkylation (major pathway) and oxidative denitrosation (minor pathway) are shown in Scheme 1. However, a reductive denitrosation pathway independent from oxidative dealkylation has also been proposed (path d in Scheme 1),[7−11] implying that the denitrosation mechanism is disputable.

Computational analysis of enzyme mechanisms such as P450 oxygenation has led to a new level of insight in the electronic structure features governing reactivity and reaction pathways.[12,13] Investigations of the alkane hydroxylation mediated by the high-valent iron-oxo P450 species known as compound I (Cpd I) with

Received: July 11, 2011
Revised: December 2, 2011
Published: December 04, 2011

Scheme 1. Major Metabolic Pathways of NDMA Catalyzed by P450s[a]

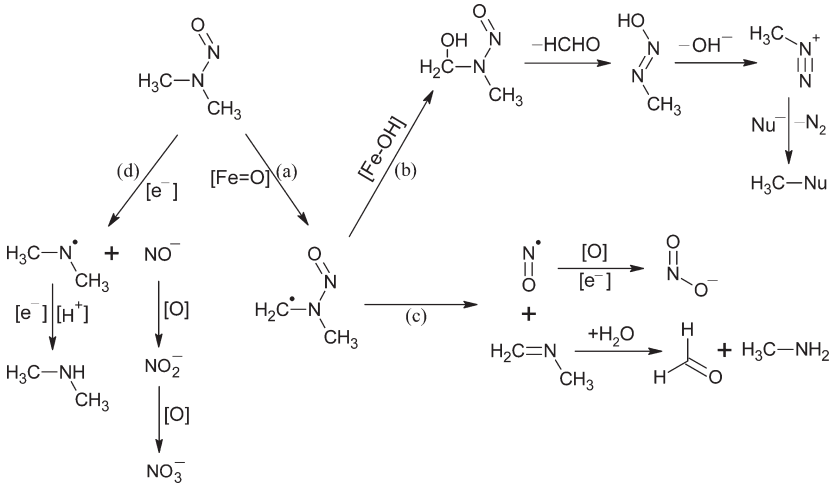

[a] Initial H-abstraction (path a) yields the α-nitrosamino radical as key intermediate for both the oxidative dealkylation (path b) and oxidative denitrosation (path c). Another assumed alternative pathway is the reductive denitrosation of NDMA (path d). Nu is an endogenous nucleophile such as a DNA base.

the quantum chemical DFT (density functional theory) method for methane[14] and propene[15] reveal that this reaction is governed by a two-state reactivity (TSR) process involving a high-spin (HS, quartet) and a low-spin (LS, doublet) pathway. While the HS reaction proceeds in a stepwise manner, the LS reaction is essentially a 1-step (concerted) process. By contrast, the Cpd I catalysis of the C–H hydroxylation of *N*,*N*-dimethylaniline proceeds mostly via the LS pathway, and both LS and HS processes are concerted.[16,17]

So far, no respective analysis had been undertaken for the α-hydroxylation of nitrosamines. In particular, it is unclear whether the TSR paradigm holds also for this reaction or whether it would proceed in a spin-selective manner. A further question is whether computational chemistry could reproduce the intrinsic KIE as observed for the dealkylation of NDMA.[4] The latter would support the H-abstraction with formation of the α-nitrosamino radical as initial reaction step of the dealkylation (path a in Scheme 1), which in turn would be the necessary condition for path c as oxidative denitrosation pathway.

In the present investigation, the α-hydroxylation (that precedes the dealkylation) and the denitrosation as two competing pathways of the metabolic conversion of NDMA through P450 are analyzed through DFT computational chemistry. The results reveal a distinct dependence of the product ratio on the LS-to-HS ratio of the overall metabolic process. Moreover, extension of the calculations to three further carcinogenic nitrosamines shows that the H-abstraction as initial step for both the dealkylation and denitrosation is energetically driven by the bond dissociation enthalpy (BDE) of the substrates, indicating a clear relationship between the metabolic rate and the α-C–H bond strength of the compounds.

COMPUTATIONAL METHODOLOGY

Level of Theory. *Gaussian 03*[18] DFT calculations were performed on the P450-catalyzed metabolism of nitrosamines, taking the six-coordinated triradicaloid oxo-ferryl complex $Fe^{4+}O^{2-}Por^{-}SH^{-}$ (Por = porphyrin ring = $C_{20}H_{12}N_4$) as model for Cpd I that in turn represents the P450 active site. Following the commonly accepted procedure for C–H hydroxylation calculations,[14−17] the unrestricted B3LYP functional (UB3LYP)[19−22] combined with the double-ζ LANL2DZ(Fe)/6-31G(H,C,N,O,S) basis set (also called LACVP; here denoted BSI) was employed for all geometry optimizations and frequency calculations, covering both the low-spin (LS, doublet) and high-spin (HS, quartet) reaction pathways. B3LYP was chosen because it yields geometries in good agreement with experimental crystal structures,[23,24] and because it correctly predicts both the doublet ground state of the resting state of P450[25] and the triplet ground state of the C_{2v} Fe(II)-porphyrin system[26,27] (with singlet and quintet states being 27.7 and 11.0 kcal/mol above the triplet state according to our current calculations).

Geometry optimization was followed by frequency calculations to confirm that all ground states had no imaginary frequency, and all transition states one. The computed vibrational frequencies were used further for quantifying the zero-point energy correction (ZPE) as well as the conversion from the electronic energy to the Gibbs free energy at 298.15 K and 101.325 kPa.

For all UB3LYP/BSI-optimized geometries, additional single-point calculations were performed at the LANL2DZ(Fe)/6-31G+** (H,C,N,O,S) level (also called LACVP+**; here denoted BSII) to obtain more accurate energies.

In order to assess the sensitivity of the calculated energies and geometries on the particular DFT functional selected, the HS quartet pathway for the rate-determining NDMA H-abstraction step was also analyzed by corresponding BP86,[28,29] BLYP,[22,28] and B3PW91[21,30] calculations. Moreover, an additional analysis of the HS NDMA H-abstraction process by Cpd I with geometry optimization on the BSI* level has been performed in order to explore the effect of polarization functions on the geometry optimization.

Solvation. Bulk polarity effects of the protein environment were evaluated with the PCM[31] approach using the united atom (UA0) cavity model through single-point calculations at the UB3LYP/BSII level with UB3LYP/BSI geometries. To explore the effect of increasing bulk polarity on the H-abstraction of NDMA by Cpd I within the ε range from 2 to 40 as discussed for

dx.doi.org/10.1021/jp206570n |*J. Phys. Chem. B* 2012, 116, 903–912

Scheme 2. Free Energy Profiles for the HS and LS α-Hydroxylation and Denitrosation of NDMA by Cpd I (Represented Computationally as $Fe^{4+}O^{2-}Por^{-}SH^{-}$) of P450, along with Bond Lengths in Å and Angles in Degree of the Key Reaction Species in the HS (LS) State[a]

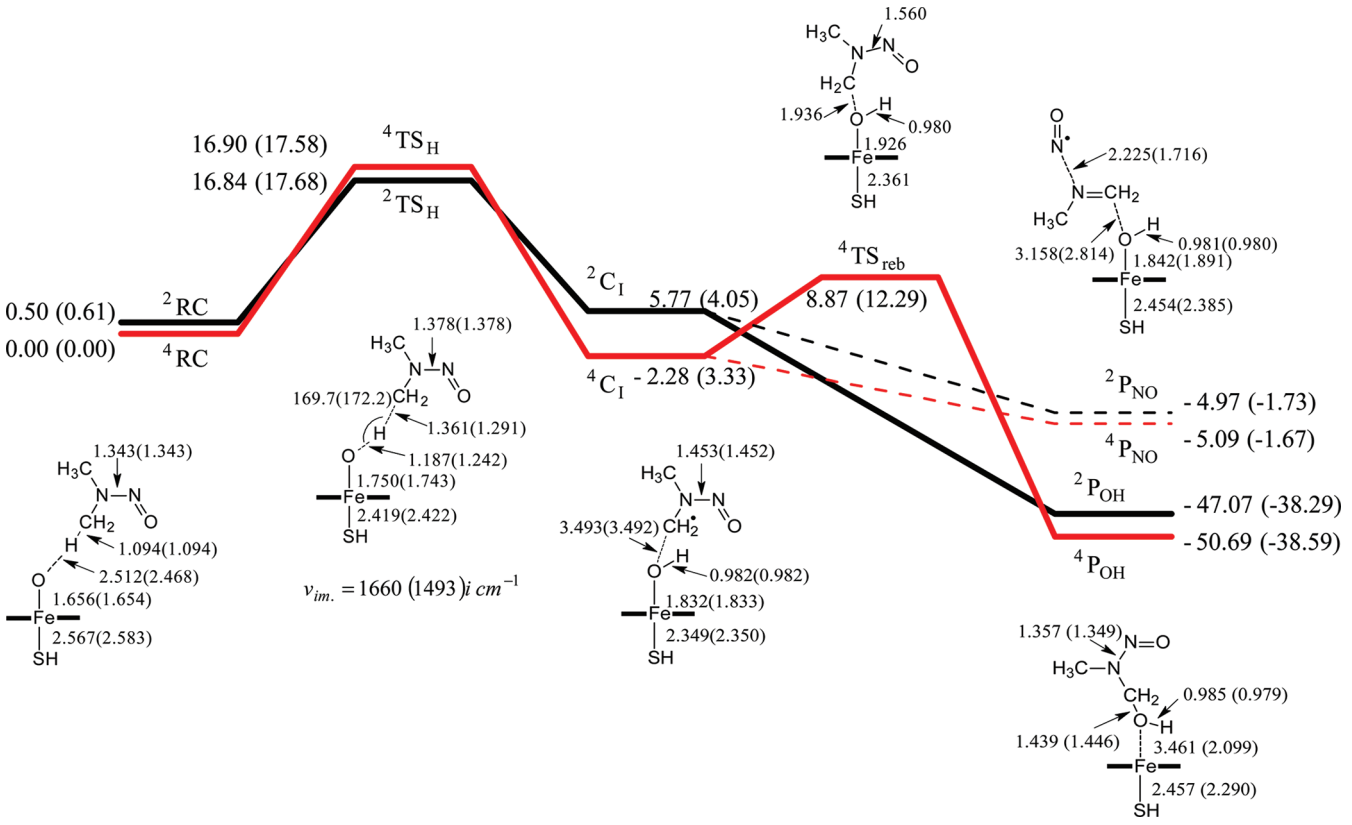

[a] Free energies [kcal/mol] at 298.15 K approximated through eq 1 are given relative to the quartet reactant complex ^{4}RC at the UB3LYP/BSII//BSI level including single-point bulk solvation (PCM/BSII, ε = 5.6); the respective gas-phase free energies confined to BSI are indicated in parentheses. ^{4,2}RC = quartet and doublet reactant complex, TS_H = transition state of H-abstraction, C_I = intermediate complex with H abstracted by Cpd I, TS_{reb} = rebound transition state, P_{OH} = hydroxylated product + Fe(PorSH), P_{NO} = nitric oxide + imine + FeOH(PorSH).

protein environments,[32,33] the following three settings have been used for respective single-point calculations: ε = 5.6 (nonpolar solvent chlorobenzene), 10.36 (dichloroethane), and 36.64 (acetonitrile).

Solution-phase free energies (G_{sol}) were estimated through combining BSII-level single-point energies including PCM solvation obtained for BSI-level geometries with BSI-level free energy corrections at 298.15 K

$$G_{sol}(298.15K) \approx E(\text{UB3LYP/BSII//BSI}) + \Delta E_{sol}(\text{UB3LYP-PCM/BSII//BSI}) + \Delta G(\text{UB3LYP/BSI}) \quad (1)$$

Reaction Rate Constant. The rate constant of an elementary reaction, k, is related to its free energy of activation, $\Delta G^{\ddagger}$, through the Eyring equation

$$k = \frac{k_B T}{h}\frac{1}{c^0}\exp\left(-\frac{\Delta G^{\ddagger}}{RT}\right) \quad (2)$$

where k_B is the Boltzmann constant, h is the Planck constant, R is the gas constant, T is the temperature in Kelvin, and c^0 is the concentration defining the standard state (typically 1 mol/L). Equation 2 was used to convert the LS-to-HS difference in $\Delta G^{\ddagger}$ into a corresponding difference in the reaction rate constant.

Kinetic Isotope Effect (KIE). The intrinsic KIE values of the hydroxylation reaction were studied using the semiclassical Eyring and Wigner models by replacing the appropriate hydrogen atoms with their deuterated counterparts.[15,34] The semiclassical Eyring model reads

$$k_H/k_D = \exp[(\Delta G_D^{\ddagger} - \Delta G_H^{\ddagger})/RT] \quad (3)$$

where $\Delta G_D^{\ddagger}$ and $\Delta G_H^{\ddagger}$ are the free energies of activation of the substrate with and without deuterium, respectively. The Wigner correction to the Eyring KIE is obtained by multiplying k_H/k_D with the tunneling ratio ($Q_{t,H}/Q_{t,D}$), where Q_t is estimated as follows:

$$Q_t = 1 + u_t^2/24 \text{ with } u_t = h\nu/k_B T \quad (4)$$

In eq 4, h is Planck's constant, k_B is the Boltzmann constant, and ν (UB3LYP/BSI frequency scaled by 0.9704[35]) is the value of the imaginary frequency in the transition state.

RESULTS AND DISCUSSION

Initial P450-Mediated H-Abstraction of NDMA. Scheme 2 shows the UB3LYP-PCM free energy profiles for the HS and LS

dx.doi.org/10.1021/jp206570n |J. Phys. Chem. B 2012, 116, 903–912

α-hydroxylation (as first part of the dealkylation pathway) and denitrosation of NDMA as catalyzed by Cpd I. Moreover, the figure informs about key bond lengths of the molecular species and their variation along the reaction coordinate.

Initially, NDMA and Cpd I form HS and LS reactant complexes, ^{4}RC and ^{2}RC, stabilized through weak H-bonding between the Fe-coordinated oxygen and one H atom of the α-methyl group of NDMA (O···H distance ∼2.5 Å), yielding a slightly higher energy for the LS state as compared to the HS state (by 0.50 kcal/mol at the solution-phase free-energy level approximated through to eq 1, employing single-point PCM with ε = 5.6 simulating bulk protein environment). Subsequent H atom transfer from C−H to the Fe^{IV}=O moiety of Cpd I is rate-determining for both the HS and LS pathways, with the former having a slightly higher reaction barrier (16.90 vs 16.34 kcal/mol). Interestingly, the HS transition state ^4TS_H is a bit later on the reaction coordinate than its LS counterpart ^2TS_H, as can be seen through comparison of their C···H and H···O distances (1.36 vs 1.29 Å and 1.19 vs 1.24 Å). Moreover, the O···H···C configuration is almost linear as for other H-abstraction transition states,[14,15] and the imaginary frequency is large as expected for an H-abstraction process.

Increasing the bulk polarity yields still very close H-abstraction barriers between HS and LS pathways (ε = 10.36, 17.02 vs 16.19 kcal/mol; ε = 36.64, 17.12 vs 15.66 kcal/mol), and overall the bulk polarity has only a small impact on the TS energies as compared to the free energy correction. The similar LS and HS reaction barriers show that the initial H-abstraction from NDMA is governed by a TSR and in this respect is similar to the C−H hydroxylation of alkanes[14,15] but different to the one found for *N*,*N*-dimethylaniline.[16,17]

While the LS and HS energies are similar for both the reactant complex and the H-abstraction TS as outlined above, the intermediate as next characteristic molecular species along the reaction coordinate is more stable by 8.05 kcal/mol in the quartet state (^4C_I = ^{4}[FeOH(PorSH) + •$CH_2N(CH_3)NO$]) than in the doublet state (^2C_I). Interestingly, ^4C_I and ^2C_I have very similar geometries including the distance between the Fe-coordinated oxygen and the α-methyl carbon (3.493 vs 3.492 Å). Note further that in the intermediate, the N−N bond length of the α-nitrosamino radical (1.45 Å) is larger by 0.07 Å than in the preceding TS and larger by 0.11 Å than in the α-nitrosamine of the initial reactant complex. This indicates that upon H-abstraction from the α-C, NDMA, and nitrosamines in general, become more ready for a homolytic cleavage of the NO unit.

Hydroxylation vs Denitrosation. From the intermediate complex (^4C_I and ^2C_I in Scheme 2), the α-nitrosamino radical either rebounds to OH to form α-hydroxynitrosamine + Fe(PorSH) in the HS or LS state ($^4P_{OH}$ and $^2P_{OH}$), or fragments with essentially no barrier for the N−N bond cleavage to yield nitric oxide + imine + FeOH(PorSH) on the denitrosation pathway ($^4P_{NO}$ and $^2P_{NO}$). At the UB3LYP/BSI level of theory, the energies of the optimized N−N bond cleavage transition states are below the ones of the preceding intermediate for both the quartet and doublet states, indicating that the denitrosation reaction barrier can be considered as being negligible.

Interestingly, the denitrosation product complexes $^4P_{NO}$ and $^2P_{NO}$ have very similar free energies (−5.09 vs −4.97 kcal/mol relative to ^{4}RC; see Scheme 2), but differ significantly with regard to both the N···N distance (2.23 vs 1.72 Å) and the imine−C···O−Fe distance (3.16 vs 2.81 Å). These findings show that the decomposition into the three subunits NO, imine and FeOH(PorSH) is much more pronounced for the HS product than for the LS product, keeping in mind that both $^4P_{NO}$ and $^2P_{NO}$ are converted further to yield NO_2 and a carbonyl (through hydrolysis of the imine) as outlined above in Scheme 1.

Coming back to the α-C hydroxylation as alternative (and for NDMA in fact preferred) follow-up reaction of the intermediate, the respective rebound step (with H−O• approaching •CH_2R) is barrier-free on the LS surface, whereas it proceeds with a significant barrier on the HS surface ($^4TS_{reb}$, 11.15 kcal/mol, $\nu_{im.}$ = 267.4*i* cm^{-1}). It follows that the TSR characteristics of the NDMA hydroxylation correspond to the ones reported for the alkane hydroxylation:[14,15] The LS pathway is concerted, while the HS reaction is a two-step process with a second TS barrier of ca. 11 kcal/mol. Nevertheless, the HS hydroxylation is thermodynamically preferred because of a slightly lower reaction free energy (−50.69 vs −47.57 kcal/mol).

According to experimental information, the denitrosation was estimated to account for only about 14−20% of the P450-catalyzed biotransformation of NDMA.[36] This implies a correspondingly strong preference for the intermediate α-nitrosamino radical to become hydroxylated ($C_I \rightarrow P_{OH}$) rather than fragmented ($C_I \rightarrow P_{NO}$). Under thermodynamic control of the overall reaction, this would concur qualitatively with our present calculation results for the reaction free energies, although the obtained difference of around 45 kcal/mol in favor of the α-hydroxylation would translate into a still much lower fraction of the denitrosation product. Considering further the fact that the LS rebound process has no reaction barrier, it is unlikely that this pathway contributes significantly to the denitrosation as thermodynamically less favorable side reaction. By contrast, the HS rebound barrier of 11.15 kcal/mol provides sufficient lifetime for the preceding α-nitrosamino radical to feed both the α-hydroxylation and denitrosation in the HS channel. These differences in kinetics between the HS and LS hydroxylation route suggest that the latter is the dominant pathway for the α-hydroxyl nitrosamine formation, keeping in mind that the quartet intermediate (^4C_I) prefers kinetically the alternative denitrosation reaction. Thus we conclude that the denitrosation products originate mainly from the HS channel with its $^4TS_{reb}$ barrier, whereas the α-hydroxylation, followed by dealkylation and subsequent alkyl diazonium ion formation (see Scheme 1 above), is mainly fed by the LS reaction pathway.

Depending on the ε value selected for the PCM solvation calculation, the ^2TS_H barrier is lower than the ^4TS_H barrier by 0.54−1.46 kcal/mol. Introduction of these values into the Eyring equation (eq 2) yields a LS:HS ratio for the associated reaction rate constant of 3 to 13. This result is compatible with the experimental finding that the ratio of the reaction rates of dealkylation vs denitrosation is 8:1 for NDMA.[37] It follows that the calculated LS:HS ratio of the H-abstraction rate constant supports our view that for NDMA the observed dealkylation to denitrosation ratio reflects the LS to HS ratio of the overall TSR process.

Kinetic Isotope Effect. The magnitude of the kinetic isotope effect (KIE) yields pertinent information about the reaction mechanism and the bond or bonds subject to change, as has been demonstrated with the C−H bond cleavage as prominent example.[38] Recently, the KIE of the *N*-dealkylation of NDMA catalyzed by cytochrome P450 2A6 has been measured to be ca. 10, indicating that deuteration of NDMA results in a 10-fold reduction of the reaction rate.[4] This result provides opportunity to test our hypothesis that the rate-determining step for the dealkylation is the initial H-abstraction yielding the α-nitrosamino radical, and that the subsequent hydroxylation through

Table 1. UB3LYP/BSI-Calculated KIE and Imaginary Frequency for the H-Abstraction from the α-C of NDMA As Catalyzed by Cpd I[a]

reacting molecular species	KIE (Eyring)	KIE (Wigner)	imaginary frequency (cm^{-1}) ν(H)	ν(D)
		HS		
$CD_2H-N(NO)-CD_2H\cdots O$ vs $CD_2H-N(NO)-CHDD\cdots O$	6.3	8.9	−1650.2*i*	−1260.0*i*
$CH_3-N(NO)-CH_2H\cdots O$ vs $CD_3-N(NO)-CD_2D\cdots O$	2.3	3.3	−1659.9*i*	−1254.5*i*
$CD_3-N(NO)-CH_2H\cdots O$ vs $CH_3-N(NO)-CD_2D\cdots O$	8.2	12.0	−1671.2*i*	−1254.6*i*
$CH_3-N(NO)-CH_2H\cdots O$ vs $CH_3-N(NO)-CD_2D\cdots O$	2.3	3.3	−1659.9*i*	−1254.6*i*
average	4.8	6.9	−1660.3*i*	−1255.9*i*
		LS		
$CD_2H-N(NO)-CD_2H\cdots O$ vs $CD_2H-N(NO)-CHD\cdots O$	6.4	9.0	−1565.7*i*	−1202.1*i*
$CH_3-N(NO)-CH_2H\cdots O$ vs $CD_3-N(NO)-CD_2D\cdots O$	5.8	7.7	−1493.1*i*	−1196.5*i*
$CD_3-N(NO)-CH_2H\cdots O$ vs $CH_3-N(NO)$-$CD_2D\cdots O$	8.0	11.4	−1589.6*i*	−1196.7*i*
$CH_3-N(NO)-CH_2H\cdots O$ vs $CH_3-N(NO)-CD_2D\cdots O$	5.8	7.7	−1493.1*i*	−1196.7*i*
average	6.5	8.9	−1535.4*i*	−1198.0*i*

[a] Cpd I was represented by $Fe^{4+}O^{2-}Por^{-}SH^{-}$; KIE = k_H/k_D, where k_H and k_D refer to the left and right NDMA species as shown in the first column (with Cpd I being indicated through its H-abstracting oxygen); HS = high spin (quartet), LS = low spin (doublet); Eyring = Eyring model (eq 3), Wigner = Eyring KIE multiplied by the Wigner tunneling factor (eq 4).

Table 2. UB3LYP/BSI-Calculated Mulliken Spin Densities for Substructural Units of the Isolated Model of Cpd I ($Fe^{4+}O^{2-}Por^{-}SH^{-}$) and the Molecular Species Involved in the P450-Mediated NDMA α-Hydroxylation and Denitrosation Processes[a]

	substructural unit and spin density								
	Cpd I ($Fe^{4+}O^{2-}Por^{-}SH^{-}$)				substrate				
molecular species	Fe	O	Por	SH	Sub•	H	CH_2	N	NO
^{4}Cpd I	1.04	0.98	0.44	0.54	n.a.	n.a.	n.a.	n.a.	n.a.
^{2}Cpd I	1.17	0.92	−0.50	−0.59	n.a.	n.a.	n.a.	n.a.	n.a.
^{4}RC	1.10	0.92	0.45	0.52	0.00	0.00	0.00	0.00	0.00
^{2}RC	1.24	0.86	−0.53	−0.57	0.00	0.00	0.00	0.00	0.00
^4TS_H	1.19	0.64	0.25	0.42	0.56	−0.06	0.40	−0.04	0.20
^2TS_H	1.83	0.09	−0.29	−0.22	−0.43	0.03	−0.29	0.00	−0.14
^4C_I	1.88	0.22	−0.12	0.02	0.99	0.01	0.53	−0.11	0.56
^2C_I	1.88	0.22	−0.13	0.01	−0.98	0.00	−0.53	0.11	−0.56
$^4TS_{reb}$	1.02	0.08	1.04	0.13	0.72	0.00	0.10	−0.06	0.68
$^4P_{OH}$	2.49	0.00	0.04	0.47	0.00	0.00	0.00	0.00	0.00
$^2P_{OH}$	1.10	0.00	−0.09	−0.02	0.00	0.00	0.00	0.00	0.00
$^4TS_{N-N}$	1.90	0.22	−0.11	0.00	0.98	0.00	0.26	−0.10	0.83
$^2TS_{N-N}$	1.86	0.21	−0.14	0.01	−0.94	0.00	−0.25	0.10	−0.79
$^4P_{NO}$	0.90	0.14	0.56	0.40	1.00	0.00	0.01	−0.03	1.02
$^2P_{NO}$	0.95	0.10	0.32	0.25	−0.60	0.00	−0.10	0.06	−0.57

[a] RC = reactant complex, TS_H = transition state of initial H-abstraction, C_I = intermediate after H-abstraction, TS_{reb} = rebound transition state, P_{OH} = hydroxylated product + Fe(PorSH), TS_{N-N} = transition state of N−N bond cleavage, P_{NO} = nitric oxide + imine + FeOH(PorSH). See Scheme 2. Sub• = α-nitrosamino radical; n.a. = not applicable.

the •OH rebound process is mainly fed by the LS pathway, while the HS state of the intermediate radical, ^4C_I, strongly prefers the alternative fragmentation into •NO and further components (see above and Scheme 2).

Table 1 summarizes our calculation results for the KIE (k_H/k_D = ratio of rate constants without and with deuterium) of the P450-mediated H-abstraction for both the HS ($^4RC \rightarrow {}^4TS_H \rightarrow {}^4C_I$) and LS ($^2RC \rightarrow {}^2TS_H \rightarrow {}^2C_I$) pathway. Application of the semiclassical Eyring model (eq 3) yields average KIE values of 4.8 (^4TS_H) and 6.5 (^2TS_H), which rise through the Wigner correction (eq 4) for tunneling to 6.9 (^4TS_H) and 8.9 (^2TS_H), respectively. The LS Wigner-corrected result comes pretty close to the experimental value, supporting our conclusion that the dealkylation proceeds mainly through the LS route. Moreover, these findings provide further evidence that the initial rate-determining step is indeed H-abstraction.

Electronic Structure Characteristics. The Fe redox states involved in the catalytic process require attention. Complexation

dx.doi.org/10.1021/jp206570n |J. Phys. Chem. B 2012, 116, 903–912

of Fe in Cpd I transforms its original d-block mainly into the five molecular orbitals δ_{xy}^2, $\pi^*_{yz}{}^1$, $\pi^*_{zx}{}^1$, $\sigma^*_{x^2-y^2}{}^0$;, and $\sigma^*_{z^2}{}^0$, resulting in oxidation state IV.[39,40] Here, the ferryl Fe^{IV}═O moiety is best described as diradicaloid triplet species, with a net dπ(Fe)−pπ(O) bond resulting from two three-electron bonds that correspond to a $\pi_{yz}{}^2\pi^*_{yz}{}^1 + \pi_{zx}{}^2\pi^*_{zx}{}^1$ occupancy.[39,40] Spin coupling with the single Por a_{2u} orbital (hence, $Por^{+\bullet}$; a_{2u} has large amplitudes at the Por N atoms) yields the ferromagnetic quartet (all three spins parallel) and the antiferromagnetic doublet (antiparallel coupling of the single Por a_{2u} electron with one of the two Fe π^* electrons) states, respectively.[40]

In Table 2, UB3LYP/BSI Mulliken spin densities are summarized for Cpd I (represented by $Fe^{4+}O^{2-}Por^{-}SH^{-}$) and the molecular species involved in the NDMA α-hydroxylation and denitrosation processes. As can be seen from the table, our present calculations yield spin densities for Cpd I at Fe, O, Por and SH of 1.04, 0.98, 0.44, and 0.54 (quartet) and 1.17, 0.92, 0.50, and 0.59 (doublet), respectively. It suggests a resonance description of Cpd I as shown in Scheme 3, visualizing the two three-electron bonds (in addition to one σ bond) between Fe and O with both atoms carrying one unpaired electron on the average, and a third single electron being delocalized between the porphyrin unit and the thiol sulfur. The latter can be rationalized through an $a_{2u}\pi$(Por)−pσ(S) interaction,[14] symbolized by $Por^{+\bullet}SH \leftrightarrow PorSH^{+\bullet}$.

In the N-dealkylation reaction of *N*,*N*-dimethylaniline by Cpd I, the developing spin density on the $\bullet CH_2$ moiety was found to be delocalized toward the nitrogen lone pair in the H-abstraction transition state.[17] This contrasts with our present findings for NDMA with calculated spin densities at $\bullet CH_2$ and the adjacent N atom of 0.40 and 0.04 (^4TS_H) and 0.29 and 0.00 (^2TS_H), respectively (Table 2). The latter is supported by the experimental finding that N nitrosation increases the N oxidation potential,[41] which could be rationalized through a reduced N electron density as compared to amino N.

In both the HS and LS intermediate ($^{4,2}C_I$), the spin density is reduced to 0.22 at O, and raised to 1.88 at Fe, with only small amounts left at Por (0.12/0.13) and SH (0.02/0.01). These results suggest a prevalence of Fe^{IV} (ferryl) over Fe^{III} (ferric) in the FeOH moiety in its intermediate complex with one H atom abstracted from NDMA, corresponding to the right resonance (electromer) form of Scheme 4. This electronic structure interpretation of the spin density distribution of C_I corresponds to the reported prevalence of Fe^{IV} electromers over Fe^{III} species for most alkane hydroxylation C_I species in the gas phase.[12,42] By contrast, the protein environment was reported[12,42] to favor the Fe^{III}-type C_I species (left resonance forms in Scheme 4) in alkane hydroxylation reactions; however, our calculations did not allow us to locate an Fe^{III} electromer, and so we cannot assess the respective Fe^{IV}−Fe^{III} energy difference within the presently selected computational framework. Interestingly, the spin density of the α-nitrosamino radical (0.99/0.98) splits mainly between the $\bullet CH_2$ (0.53) and NO (0.56) moieties, the latter of which reflects again its increased readiness for cleaving •NO as detoxification process.

The above-mentioned substantial difference in the geometry between the HS and LS denitrosation products ($^4P_{NO}$ and $^2P_{NO}$) is reflected in their spin densities. In particular, NO carries a full unpaired electron only in $^4P_{NO}$ (HS vs LS NO spin density: 1.02 vs 0.57), providing further support for the HS pathway as main source of the denitrosation.

Relationship between H-Abstraction Barrier and Substrate BDE. While the initial H-abstraction from the α-C of NDMA is catalyzed by P450, the associated reaction barrier is still related to the C−H bond strength. It follows that when comparing different α-CH_n-nitrosamine substrates, their H-abstraction barriers should correlate with their C−H bond dissociation enthalpies. In order to test this assumption, we

Scheme 3. Major Resonance Forms of Ferryl Cpd I[a]

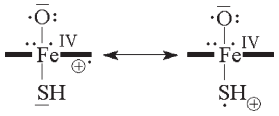

[a] The porphyrin unit is represented by two hyphens connected to Fe (—Fe—).

Scheme 4. Resonance Forms of the Intermediate Complex C_I of Cpd I after H Abstraction from NDMA[a]

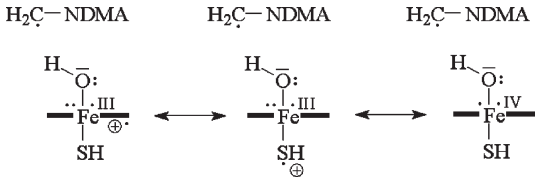

[a] Left and middle: ferric (Fe^{III}) complex. Right: ferryl (Fe^{IV}) complex.

Scheme 5. Key Geometric Features[a] and the Imaginary Frequencies of UB3LYP/BSI Optimized $^{4(2)}TS_H$ Species for the H-Abstraction Transition States of NNN (left), NPYR (middle), and NMVA (right) with Cpd I of P450

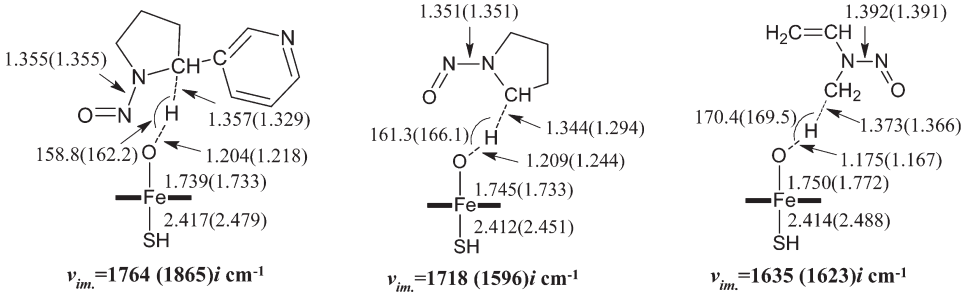

[a] Lengths in Å and angles in degrees.

dx.doi.org/10.1021/jp206570n | *J. Phys. Chem. B* 2012, 116, 903–912

Table 3. H-Abstraction Barrier TS_H Relative to Separated Reactants (^{4,2}Cpd I + Nitrosamine) and Bond Dissociation Enthalpy for the α-C−H Bond (BDE_{C-H}) of the Isolated Nitrosamines[a]

	TS_H [kcal/mol]						
	HS		LS		spin-averaged		
compound	$\Delta E^{\ddagger}$	$\Delta G^{\ddagger}$	$\Delta E^{\ddagger}$	$\Delta G^{\ddagger}$	$\Delta E^{\ddagger}_{av}$	$\Delta G^{\ddagger}_{av}$	BDE_{C-H} [kcal/mol]
NNN	10.97	20.11	9.83	18.14	10.40	19.12	78.98
NPYR	11.89	21.11	11.69	20.38	11.79	20.75	83.21
NDMA	12.82	21.58	13.53	21.30	13.18	21.44	86.30
NMVA	13.91	21.40	14.41	22.43	14.16	21.91	87.22

[a] H-abstraction barriers without and with free energy correction for 298.15 K were calculated at the UB3LYP/BSI level (for BSI see section Computational Methodology), and BDE_{C-H} at 298.15 K was obtained from UB3LYP/6-311++G** calculations according to eq 5 (see text).

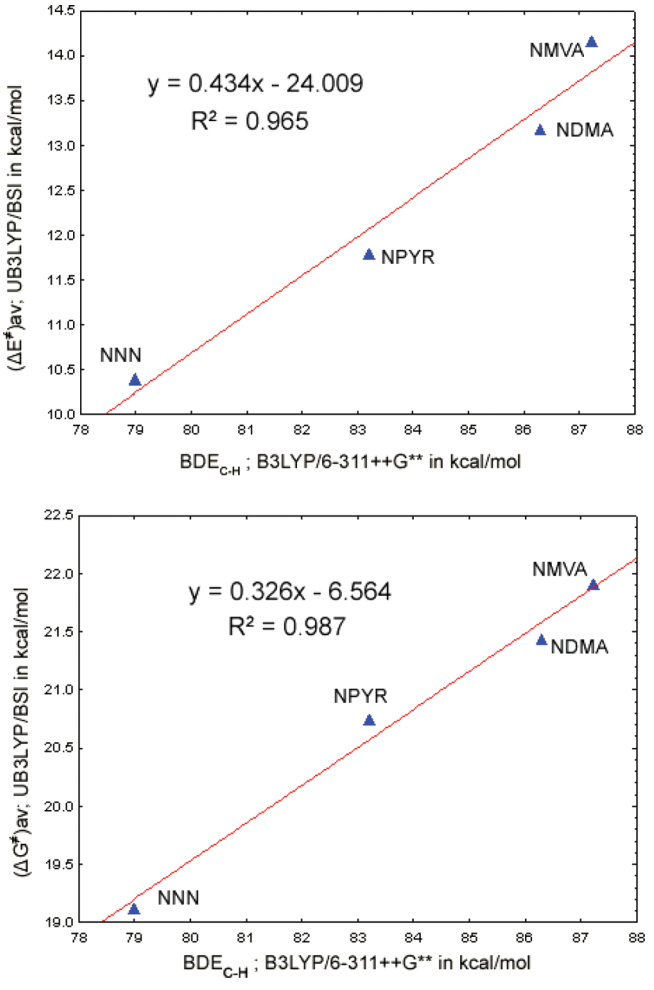

Figure 1. Two-spin (doublet, quartet) averaged H-abstraction energy barrier $\Delta E^{\ddagger}$ (top) and free energy barrier $\Delta G^{\ddagger}$ (bottom) in kcal/mol vs C−H bond dissociation enthalpy (BDE_{C-H} at 298 K in kcal/mol) for the four α-CH_n-nitrosamines NNN, NPYR, NDMA, and NMVA.

have extended our H-abstraction barrier analysis to *N*-nitroso-*N*-methylvinylamine (NMVA),[43] *N*-nitrosopyrrolidine (NPYR),[44] and *N*′-nitrosonornicotine (NNN)[45] and performed additional BDE (298.15 K) calculations at the 6-311++G** level for all four nitrosamines as isolated substrates employing eq 5

Table 4. Calculated Ionization Potential (IP) Energies (eV) for the α-Nitrosamino Radical of NDMA, NNN, NPYR, and NMVA at B3LYP/6-311++G and B3LYP/6-31G level**

	IP energy (eV)	
α-nitrosamino radical	B3LYP/6-311++G**	B3LYP/6-31G
NDMA	7.06	6.86
NNN	6.55	6.33
NPYR	6.75	6.53
NMVA	6.97	6.77

(where H = enthalpy at 298.15 K)

$$BDE_{C-H}(298.15\ K) = H(R\bullet) + H(H\bullet) - H(R\text{–}H) \quad (5)$$

For NNN, NPYR, and NMVA, the chemical structures and key geometric features of their P450-mediated H-abstraction TS in the HS and LS state are summarized in Scheme 5. As already found for the TS of NDMA, the α-C···H distance is larger (^4TS_H, 1.34−1.37 Å; ^2TS_H, 1.29−1.37 Å) than the H···O(Fe) distance (^4TS_H, 1.18−1.21 Å; ^2TS_H, 1.17−1.24 Å), indicating a more product-like TS. Similarly, the calculated imaginary frequencies (1596−1865 cm^{-1}; Scheme 5) are similar to the ones obtained for NDMA (1493−1660 cm^{-1}; see Scheme 2), confirming the C−H bond breaking process as rate-determining step.

Table 3 lists both the H-abstraction barriers (energy barrier $\Delta E^{\ddagger}$ and free energy barrier $\Delta G^{\ddagger}$) and BDE_{C-H} values for all four α-CH_n-nitrosamines. Interestingly, the HS energy barrier is below the LS energy barrier for NDMA and NMVA, but above the LS energy barrier for NNN and NPYR. Concerning $\Delta G^{\ddagger}$, the HS value is below the LS value only for NMVA. Overall the HS:LS energy barrier difference varies from 1.14 kcal/mol (NNN) to −0.71 kcal/mol (NDMA), whereas the corresponding free energy barrier difference varies from 1.97 kcal/mol (NNN) to −1.03 kcal/mol (NMVA). Nevertheless, the variation in $\Delta E^{\ddagger}$ and $\Delta G^{\ddagger}$ across all four compounds shows a good correlation between the HS and LS values.

The relationship between the H-abstraction barrier (averaged over both spin states for $\Delta E^{\ddagger}$ and $\Delta G^{\ddagger}$) and BDE_{C-H} of the isolated substrates is shown in Figure 1. In accord with previous findings obtained for the P450-catalyzed alkane hydroxylation,[46,47] the plots reveal a significant correlation between both properties, indicating that differences in substrate BDE_{C-H} translate into

dx.doi.org/10.1021/jp206570n | J. Phys. Chem. B 2012, 116, 903–912

Table 5. Bond Lengths and Angles of the Geometry-Optimized HS H-Abstraction Transition State (^4TS_H) of NDMA + Cpd I ($Fe^{4+}O^{2-}Por^{-}SH^{-}$) with Different DFT Functionals Employing the BSI Basis Set

	interatomic distance [Å]				3-atom angle [degree]	
functional	α-C···H	H···O(Fe)	Fe···O	Fe···S	α-C···H···O	Fe···S···H
B3LYP	1.361	1.187	1.750	2.419	169.663	98.068
BP86	1.367	1.207	1.762	2.377	170.346	97.574
BLYP	1.390	1.195	1.778	2.429	170.585	98.237
B3PW91	1.334	1.207	1.738	2.361	169.443	97.713

differences in the P450-catalyzed H-abstraction rate in an inversely proportional manner. At present, we are not aware of experimental data suitable for checking the predicted increase in H-abstraction $\Delta G^{\ddagger}$ in the order NNN, NPYR, NDMA, and NMVA. However, it was concluded earlier that as the substrate radical is becoming a better electron donor (lower ionization potential (IP) energy), the HS rebound barrier will gradually decrease and may even vanish in some extreme cases.[34]

The IP energies for the α-nitrosamino radicals of NDMA, NNN, NPYR, and NMVA are listed in Table 4. Among these four α-nitrosamine radicals, NNN is the best electron donor with the lowest IP energy and thus should show the lowest HS rebound free energy barrier. Indeed, the calculated free energy $^4TS_{reb}$ barrier of NNN (UB3LYP/BSI, 3.32 kcal/mol with $\nu_{im.}$ = 381*i* cm^{-1}; PCM-UB3LYP/BSII//BSI, 2.89 kcal/mol with ε = 5.6) is much lower than the one of NDMA (gas-phase, 8.96 kcal/mol; PCM, 11.15 kcal/mol) as poorest electron donor. Interestingly, NNN as a most studied tobacco-specific nitrosamine was reported to also undergo direct denitrosation to nornicotine.[48] In view of the present computational analysis, this finding is in accord with a finite rebound barrier that makes the denitrosation pathway feasible as side-product route. As such, the TSR scenario appears reasonable to account for the oxidative metabolism of nitrosamines by cytochrome P450 enzymes.

Variation of DFT Functional and Basis Set Size. As mentioned above, the HS transition state for the initial H-abstraction, ^4TS_H, has been used to explore the dependence of the calculated geometry on the choice of the DFT functional. To this end, additional geometry optimizations for ^4TS_H have been performed with the functionals BP86, BLYP, and B3PW91. In Table 5, the results are compared for key bond lengths and angles with the ones from B3LYP. Overall, there are only minor variations across the four functionals with somewhat more pronounced changes for the weak coordinative bond Fe···S, and in any case there is no qualitative change of the TS geometry. In line with previous investigations,[23−25] these results provide further confidence in the major geometric features along the reaction coordinate (Scheme 2) as obtained with B3LYP.

Finally, the P450-catalyzed HS H-abstraction from NDMA was comparatively analyzed at the UB3LYP/BSII//BSI* level in order to evaluate the potential effect of polarization functions on both the ^4TS_H barrier and geometry. Addition of bulk solvation (PCM with ε = 5.6) and the free energy correction resulted in a difference for $\Delta G^{\ddagger}$ of only about 0.1 kcal/mol as compared to the UB3LYP/BSII//BSI level. Moreover, the BSI*-optimized ^4TS_H geometry is very similar to its BSI-derived counterpart, with differences in the interatomic distances below 0.007 Å. These results are in line with previous findings,[49] where a full geometry optimization with the LACV3P+* basis set for the P450-catalyzed epoxidation gave only minor geometric and energetic differences to those obtained with the smaller basis set LACVP (that corresponds to our BSI). It follows that for DFT computational chemistry analyses of substrate oxidations catalyzed by Cpd I, BSI without polarization functions appears to be sufficient for generating reasonable geometries for both ground and transition states.

Reductive Denitrosation Pathways. Building on spectroscopic evidence for a P450-NO complex,[7] Appel and co-workers suggested that the N atom of the nitroso moiety of nitrosamines could directly bind to the ferric center of cytochrome P450, with subsequent homolytic cleavage of the respective secondary amine

$$Por{-}Fe^{3+}\cdots N(=O)NR_2 + 2e^- + H^+ \rightarrow Por{-}Fe^{2+}\cdots NO + R_2NH \quad (6)$$

followed by an O_2/NO ligand exchange to yield $Por{-}Fe^{2+}\cdots O_2$ and NO (the latter of which is transformed further via NO_2^- to NO_3^-).[10,11] Recently, this hypothesis got further support through the detection of some nitrosamine adducts of synthetic iron porphyrins.[50] However, present UB3LYP/BSI calculations indicate a repulsive interaction between the nitroso N of NDMA and both ferric and ferrous Fe of the respective pentacoordinated Fe−Por complexes in their HS ground states (sextet for $Por{-}Fe^{3+}$, and quintet for $Por{-}Fe^{2+}$).[42] A similar repulsive interaction is also calculated for the corresponding HS O-binding configurations $Por{-}Fe^{3+}\cdots O{=}N{-}N(CH_3)_2$ and $Por{-}Fe^{2+}\cdots O{=}N{-}N(CH_3)_2$, respectively. These results suggest that respective complexes between ground-state porphyrin iron and aliphatic nitrosamines are energetically not feasible for both the N-binding and O-binding mode. By contrast, both binding modes yield weakly bound complexes between NDMA and the LS states of ferric and ferrous porphyrin (doublet for $Por{-}Fe^{3+}$ and singlet for $Por{-}Fe^{2+}$), with ferric and ferrous Fe···N distances of 2.59 and 2.11 Å and corresponding Fe···O distances of 2.15 and 2.03 Å, respectively (see Figure S1 of the Supporting Information). However, the calculated complex binding energies at the UB3LYP/BSI level in kcal/mol without and with basis set superposition error (BSSE) corrections using the counterpoise method[51] of only −4.21/2.16 ($Fe^{3+}\cdots N$), −3.10/4.76 ($Fe^{2+}\cdots N$), −7.99/−0.77 ($Fe^{3+}\cdots O$), and −2.53/4.63 ($Fe^{2+}\cdots O$) make a reductive denitrosation according to eq 6 or through the corresponding O-binding mode unlikely (note that in three of four cases, BSSE predicts the complex to be even less stable than the sum of the isolated components).

An alternative pathway for the hypothesized reductive denitrosation could be initiated through a single-electron transfer (SET) to NDMA mediated by NADPH P450 reductase, yielding either the NDMA radical anion as intermediate

or, in a concerted manner, $(CH_3)_2N\bullet$ and NO^- as direct products

$$R_2N{-}N{=}O + e^- \rightarrow R_2N{-}N{=}O^{\bullet -} \quad (7)$$

$$R_2N{-}N{=}O + e^- \rightarrow R_2NO^{\bullet} + NO^- \quad (8)$$

(path d in Scheme 1). Indeed, the catalytic cycle of P450s includes two SET processes[12,42] that might provide opportunity for respective side reactions. First, the pentacoordinated ferric porphyrin complex accepts one electron from a reductase protein, leading to a high-spin ferrous porphyrin complex. Second, after uptake of O_2 the ferrous dioxygen complex is reduced to the ferric peroxo complex.

However, NDMA is a relatively poor electron acceptor, as can be seen from its B3LYP/aug-cc-pVTZ-calculated low electron affinity (EA) of 0.18 eV in the gas phase and 0.98 eV in simulated solution (single-point PCM, ε = 5.6), and thus unlikely to compete successfully with the above-mentioned iron-porphyrin complexes for the single electrons delivered by the reductase. The latter is supported by the experimental finding that incubation of nitrosamines with NADPH P450 reductase alone did not yield denitrosation products,[11] demonstrating that generation of the latter requires the presence of P450 monooxygenases. Moreover, increasing the reductase-to-P450 ratio did not favor denitrosation,[52] again suggesting that denitrosation would depend on P450 monooxygenases.

In an attempt to explore the possible role of P450 for catalyzing a reductive denitrosation according to eqs 7 (stepwise) or 8 (concerted), we calculated the respective free energy activation barriers $\Delta G^{\ddagger}$ with Cpd I and NDMA as reaction partners. To this end, the Marcus−Hush model[53−55] was employed for the stepwise mechanism, and Savéant's model[56] for the concerted fragmentation into $(CH_3)_2N\bullet$ and NO^-, both at the UB3LYP/BSI level of theory (for details see the Supporting Information). The accordingly obtained $\Delta G^{\ddagger}$ values are very large (266 kcal/mol stepwise vs 172 kcal/mol concerted), ruling out the possibility of a SET to NDMA mediated by Cpd I.

Overall, the present analysis suggests that as opposed to previous hypotheses,[7−11] a reductive denitrosation pathway is unlikely to compete to a relevant extent with the oxidative denitrosation route, and that the latter proceeds through formation of an α-nitrosamino radical as initial metabolite for both the denitrosation and dealkylation as described above.

CONCLUSIONS

The good reproduction of the KIE experimentally determined for the P450-catalyzed dealkylation of the carcinogen NDMA by our present DFT calculations provides confidence in the level of theory employed for the computational analysis of the low-spin and high-spin metabolic conversion of this substrate. Our B3LYP results yield evidence that for NDMA, both the P450-mediated dealkylation and denitrosation proceed through an initially formed α-nitrosamino radical as first oxidative step subject to TSR, and that its dealkylation (toxification) vs denitrosation (detoxification) product ratio is mainly driven by the doublet/quartet ratio of the overall TSR process. Moreover, the calculated spin densities of Fe, O(Fe), the porphyrin unit and the thiol ligand suggest that in the intermediate complex after H-atom transfer from NDMA to Cpd I (the catalytic center of P450), the iron in the FeOH moiety is prevalent as Fe^{IV} (ferryl iron) rather than as Fe^{III} (ferric iron). Extension of the analyses to three further α-CH_n-nitrosamines shows that the substrate BDE of the reactive C−H unit governs the ultimate metabolic turnover rate. Finally, our calculations suggest that for aliphatic nitrosamines, reductive pathways of denitrosation appear to be not competitive to the oxidative denitrosation catalyzed by cytochrome P450.

ASSOCIATED CONTENT

Supporting Information. Full citation for ref 18. Total energies, free energies, and energies with zero-point energy corrections for all molecular species. UB3LYP/BSI-calculated Mulliken group charges for NDMA during the α-hydroxylation and denitrosation processes by Cpd I of P450, and Mulliken spin densities and group charges of H-abstraction transition states for NNN, NPYR, and NMVA as catalyzed by Cpd I of P450. UB3LYP/BSI calculated free energies for the nondeuterated and the deuterated reactant complexes and transition states in the NDMA KIE calculation. Figure of geometry-optimized complexes between NDMA and low-spin porphyrins. Full description of the estimation the activation free-energy barriers for the one-electron reductive denitrosation of NDMA catalyzed by Cpd I using Marcus−Hush theory and Savéant's model. Cartesian coordinates of all structures discussed in this work. This material is available free of charge via the Internet at http://pubs.acs.org.

AUTHOR INFORMATION

Corresponding Author

*Tel: +49-341-235-1262. Fax: +49-341-235-1785. E-mail: gerrit.schuurmann@ufz.de.

ACKNOWLEDGMENT

We thank Dr. Sam P. de Visser for helpful discussions regarding the computational method of our work. This work was supported by the China Scholarship Council (No. 2008619025) and the EU project OSIRIS (No. GOCE-CT-2007-037017).

REFERENCES

(1) Guengerich, F. P. *Pharmacol. Ther.* **1992**, *54*, 17–61.
(2) Lijinsky, W. *Cancer Metast. Rev.* **1987**, *6*, 301–356.
(3) Lu, X. F.; Heilman, J. M.; Blans, P.; Fishbein, J. C. *Chem. Res. Toxicol.* **2005**, *18*, 1462–1470.
(4) Chowdhury, G.; Calcutt, M. W.; Guengerich, F. P. *J. Biol. Chem.* **2010**, *285*, 8031–8044.
(5) Wade, D.; Yang, C. S.; Metral, C. J.; Roman, J. M.; Hrabie, J. A.; Riggs, C. W.; Anjo, T.; Keefer, L. K.; Mico, B. A. *Cancer Res.* **1987**, *47*, 3373–3377.
(6) Guengerich, F. P. *Chem. Res. Toxicol.* **2001**, *14*, 611–650.
(7) Appel, K. E.; Ruf, H. H.; Mahr, B.; Schwarz, M.; Rickart, R.; Kunz, W. *Chem. Biol. Interact.* **1979**, *28*, 17–33.
(8) Amelizad, Z.; Appel, K. E.; Oesch, F.; Hildebrandt, A. G. *J. Cancer Res. Clin.* **1988**, *114*, 380–384.
(9) Scheper, T.; Appel, K. E.; Schunack, W.; Somogyi, A.; Hildebrandt, A. G. *Chem. Biol. Interact.* **1991**, *77*, 81–96.
(10) Appel, K. E.; Ruhl, C. S.; Hildebrandt, A. G. *Chem. Biol. Interact.* **1985**, *53*, 69–76.
(11) Appel, K. E.; Graf, H. *Carcinogenesis* **1982**, *3*, 293–296.
(12) Shaik, S.; Cohen, S.; Wang, Y.; Chen, H.; Kumar, D.; Thiel, W. *Chem. Rev.* **2010**, *110*, 949–1017.
(13) Lonsdale, R.; Ranaghan, K. E.; Mulholland, A. J. *Chem. Commun.* **2010**, *46*, 2333–2512.
(14) Ogliaro, F.; Harris, N.; Cohen, S.; Filatov, M.; de Visser, S. P.; Shaik, S. *J. Am. Chem. Soc.* **2000**, *122*, 8977–8989.

(15) de Visser, S. P.; Ogliaro, F.; Sharma, P. K.; Shaik, S. *J. Am. Chem. Soc.* **2002**, *124*, 11809–11826.
(16) Wang, Y.; Kumar, D.; Yang, C. L.; Han, K. L.; Shaik, S. *J. Phys. Chem. B* **2007**, *111*, 7700–7710.
(17) Li, C. S.; Wu, W.; Cho, K. B.; Shaik, S. *Chem.—Eur. J.* **2009**, *15*, 8492–8503.
(18) Frisch, M. J.; et al. *Gaussian 03*, revision C.02; Gaussian, Inc.: Wallingford, CT, 2004.
(19) Becke, A. D. *J. Chem. Phys.* **1992**, *96*, 2155–2160.
(20) Becke, A. D. *J. Chem. Phys.* **1992**, *97*, 9173–9177.
(21) Becke, A. D. *J. Chem. Phys.* **1993**, *98*, 5648–5652.
(22) Lee, C. T.; Yang, W. T.; Parr, R. G. *Phys. Rev. B* **1988**, *37*, 785–789.
(23) Strickland, N.; Harvey, J. N. *J. Phys. Chem. B* **2007**, *111*, 841–852.
(24) Huang, M. J.; Liao, M. S.; Watts, J. D. *J. Comput. Chem.* **2006**, *27*, 1577–1592.
(25) Schoneboom, J. C.; Thiel, W. *J. Phys. Chem. B* **2004**, *108*, 7468–7478.
(26) Goff, H.; La Mar, G. N.; Reed, C. A. *J. Am. Chem. Soc.* **1977**, *99*, 3641–3646.
(27) Collman, J. P.; Hoard, J. L.; Kim, N.; Lang, G.; Reed, C. A. *J. Am. Chem. Soc.* **1975**, *97*, 2676–2681.
(28) Becke, A. D. *Phys. Rev. A* **1988**, *38*, 3098–3100.
(29) Perdew, J. P. *Phys. Rev. B* **1986**, *33*, 8822–8824.
(30) Perdew, J. P.; Chevary, J. A.; Vosko, S. H.; Jackson, K. A.; Pederson, M. R.; Singh, D. J.; Fiolhais, C. *Phys. Rev. B* **1992**, *46*, 6671–6687.
(31) Miertus, S.; Scrocco, E.; Tomasi, J. *Chem. Phys.* **1981**, *55*, 117–129.
(32) Honig, B.; Nicholls, A. *Science* **1995**, *268*, 1144–1149.
(33) Schutz, C. N.; Warshel, A. *Proteins* **2001**, *44*, 400–417.
(34) Kumar, D.; de Visser, S. P.; Sharma, P. K.; Cohen, S.; Shaik, S. *J. Am. Chem. Soc.* **2004**, *126*, 1907–1920.
(35) Witek, H. A.; Morokuma, K. *J. Comput. Chem.* **2004**, *25*, 1858–1864.
(36) Streeter, A. J.; Nims, R. W.; Sheffels, P. R.; Heur, Y. H.; Yang, C. S.; Mico, B. A.; Gombar, C. T.; Keefer, L. K. *Cancer Res.* **1990**, *50*, 1144–1150.
(37) Yang, C. S.; Smith, T. J.; Hong, J. Y; Zhou, S. Q. *The Chemistry and Biochemistry of Nitrosamines and Related N-Nitroso Compounds*; Loeppky, R. N., Michejda, C. J., Eds.; ACS Symposium Series 553; American Chemical Society: Washington, DC, 1994; Chapter 14, pp 169−178.
(38) Nelson, S. D.; Trager, W. F. *Drug Metab. Dispos.* **2003**, *31*, 1481–1498.
(39) Shaik, S.; Kumar, D.; de Visser, S. P. *J. Am. Chem. Soc.* **2008**, *130*, 10128–10140.
(40) Chen, H.; Lai, W. Z.; Shaik, S. *J. Phys. Chem. B* **2011**, *115*, 1727–1742.
(41) Kupper, R.; Hilton, B. D.; Kroegerkoepke, M. B.; Koepke, S. R.; Michejda, C. J. *J. Org. Chem.* **1984**, *49*, 3781–3784.
(42) Shaik, S.; Kumar, D.; de Visser, S. P.; Altun, A.; Thiel, W. *Chem. Rev.* **2005**, *105*, 2279–2328.
(43) Okazaki, O.; Persmark, M.; Guengerich, F. P. *Chem. Res. Toxicol.* **1993**, *6*, 168–173.
(44) Wong, H. L.; Murphy, S. E.; Hecht, S. S. *Chem. Res. Toxicol.* **2003**, *16*, 1298–1305.
(45) Hecht, S. S. *Chem. Res. Toxicol.* **2008**, *21*, 160–171.
(46) de Visser, S. P.; Kumar, D.; Cohen, S.; Shacham, R.; Shaik, S. *J. Am. Chem. Soc.* **2004**, *126*, 8362–8363.
(47) de Visser, S. P. *J. Am. Chem. Soc.* **2010**, *132*, 1087–1097.
(48) McIntee, E. J.; Hecht, S. S. *Chem. Res. Toxicol.* **2000**, *13*, 192–199.
(49) Kumar, D.; Karamzadeh, B.; Sastry, G. N.; de Visser, S. P. *J. Am. Chem. Soc.* **2010**, *132*, 7656–7667.
(50) Xu, N.; Goodrich, L. E.; Lehnert, N.; Powell, D. R.; Richter-Addo, G. B. *Inorg. Chem.* **2010**, *49*, 4405–4419.
(51) Boys, S. F.; Bernardi, F. *Mol. Phys.* **1970**, *19*, 553–566.
(52) Lorr, N. A.; Tu, Y. Y.; Yang, C. S. *Carcinogenesis* **1982**, *3*, 1039–1043.
(53) Marcus, R. A. *J. Chem. Phys.* **1965**, *43*, 679–701.
(54) Hush, N. S. *Trans. Faraday Soc.* **1961**, *57*, 557–580.
(55) Marcus, R. A.; Sutin, N. *Biochim. Biophys. Acta* **1985**, *811*, 265–322.
(56) Saveant, J. M. *Acc. Chem. Res.* **1993**, *26*, 455–461.